Interaction-Driven Surface Chern Insulator in Nodal Line Semimetals

Wei Chen[1,2] and J. L. Lado[1]

[1]*Institute for Theoretical Physics, ETH Zurich, 8093 Zurich, Switzerland*
[2]*College of Science, Nanjing University of Aeronautics and Astronautics, Nanjing 210016, China*

Nodal line semimetals are characterized by nontrivial bulk-band crossings, giving rise to almost flat drumheadlike surface states (DSS), which provide an attractive playground where interaction can induce symmetry-broken states and potential emergent phases. Here, we show that electronic interaction drives a Stoner ferromagnetic instability in the DSS while the bulk remains nonmagnetic, which together with spin-orbit coupling drive the surface states into a 2D Chern insulator. We show that each piece of DSS carries a half-integer topological charge, which for systems containing two pieces of DSS yield a net Chern number $\mathcal{C} = -1$. We show that this phenomenology is robust against chiral-symmetry breaking, which gives a finite dispersion to the DSS. Our results show that nodal line semimetals are a promising platform to implement surface Chern insulators and dissipationless electron transport by exploiting enhanced interaction effects of the DSS.

Topological electronic states have motivated large research efforts due to their gapped bulk coexisting with protected gapless surface modes [1–7]. In particular, chiral edge states are especially attractive as they would yield unidirectional channels lacking electric loss, representing a cornerstone in low consumption electronics. Natural compounds for Chern insulators have been proven to be rather elusive, motivating several proposals for its realization [8–11], yet the most successful implementation requires a building block that is also very rare in nature: magnetically doped topological insulators [12–14]. Thus, a key question is whether or not Chern insulators can be engineered by means of a family of materials more common in nature, which would open new possibilities in condensed matter research, apart from applications in low consumption electronics.

During the last years, the classification of topological insulators has been extended to so-called topological semimetals [15,16], i.e., systems that are gapless in the bulk and simultaneously host topologically protected surface states. The topological band crossing may occur at discrete points or along closed loops in reciprocal space. The former case corresponds to Weyl or Dirac semimetals [17–20], whereas the latter is referred as nodal line semimetals (NLSMs) [21–47]. The nodal line carries a π Berry flux [21], resulting in drumheadlike surface states (DSS) [26]. In the presence of chiral symmetry, such DSS are perfectly flat, so that any residual electronic interaction would overcome the surface kinetic energy, providing a perfect platform to realize strongly correlated and symmetry-broken surface states [48–52]. Very recently, the spontaneous magnetization in the flat band of a zigzag graphene nanoribbon was observed [53–56], indicating that the same physics may exist in the DSS, a higher-dimensional analogy of the 1D flat band in graphene nanoribbon [57].

In this Letter, we show that a surface 2D Chern insulator can emerge from electronic interaction in an NLSM. For the sake of concreteness, we focus on the NLSM containing two disconnected pieces of DSS with spin degeneracy; see Fig. 1(a). Electronic interaction results in Stoner instability in the DSS and induces a surface ferromagnetic order. The emergent exchange field together with the spin-orbit
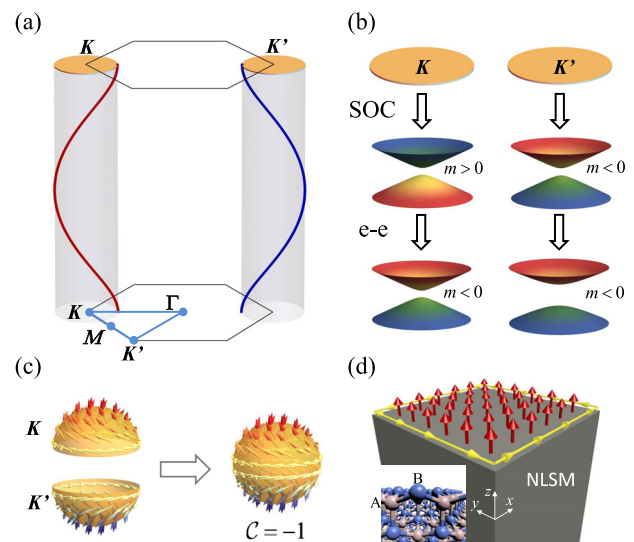

FIG. 1. (a) Nodal lines around K, K' points and corresponding DSS (light-orange disks) enclosed by their projection onto the surface Brillouin zone. (b) Spin-orbit coupling (SOC) introduces opposite mass terms to the DSS around K, K'. Electronic interaction (*e-e*) inverts one of the bands. (c) Two pieces of DSS each carries a meron spin texture with a half-integer topological charge and together constitute a Skyrmion and result in a Chern number $\mathcal{C} = -1$. (d) Spin polarized surface states and chiral hinge current. Inset: diamond lattice with an open surface.

coupling (SOC) on an open surface yield a half-integer topological charge for each piece of DSS, driving the surface band into a Chern insulator, see Figs. 1(b), 1(c). Such a spontaneously emergent 2D Chern insulator on the surface of a 3D sample would manifest in 1D chiral hinge states; see Fig. 1(d). Recent experimental progress on fabrication and detection of the ferromagnetic surface states of topological insulators paves the way to the realization of our scheme by using state-of-the-art techniques [58–61]. Our proposal highlights that NLSMs hosting two nodal lines that develop a trivial gap with SOC [57] are ideal candidates to realize a Chern insulator. In particular, spinel compounds with chemical composition XY_2Z_4 are ideal candidates in this line, as the X sites form a diamond lattice, a paradigmatic example of a system hosting two nodal lines [62].

The surface Chern insulator outlined above can be constructively derived by a concrete model of NLSM on a diamond lattice whose Hamiltonian is

$$H = H_0 + H_{\text{SOC}} + H_U, \tag{1}$$

where H_0 captures the NLSM, H_{SOC} is the intrinsic SOC and H_U is the local Coulomb interaction term that we will discuss in detail below. The Bloch Hamiltonian for the NLSM is $H_0 = d_x(\mathbf{k})\sigma_x + d_y(\mathbf{k})\sigma_y$ with $d_x(\mathbf{k}) = t + t'\cos(\mathbf{k}\cdot\mathbf{a}_3) + t\sum_{i=1}^{2}\cos(\mathbf{k}\cdot\mathbf{a}_i)$ and $d_y(\mathbf{k}) = t'\sin(\mathbf{k}\cdot\mathbf{a}_3) + t\sum_{i=1}^{2}\sin(\mathbf{k}\cdot\mathbf{a}_i)$, where Pauli matrices $\sigma_{x,y}$ act on the AB sublattice space [inset in Fig. 1(d)], t, t' are the nearest-neighbor hopping, and t' denotes the hopping along the (1,1,1) orientation, which has been set to the z axes for simplicity. The corresponding lattice vectors are $\mathbf{a}_1 = a[1/(2\sqrt{2}), \sqrt{3}/(2\sqrt{2}), 0]$, $\mathbf{a}_2 = a[-1/(2\sqrt{2}), \sqrt{3}/(2\sqrt{2}), 0]$, $\mathbf{a}_3 = a[0, \sqrt{6}/6, \sqrt{3}/3]$, with a being the lattice constant. When $t'/t < 1$, the system is an NLSM, carrying two spiral nodal lines. In a thick two-dimensional slab, the nodal lines get projected around $\mathbf{K} = [-4\sqrt{2}\pi/(3a), 0]$ and $\mathbf{K}' = -\mathbf{K}$ in the $k_x - k_y$ plane of the two-dimensional Brillouin zone [24,69–71]; see Fig. 1(a). This can be seen in the limiting case $t' \to 0$ by expanding H_0 around $\pm\mathbf{K}$ points as $h^\pm = d_x^\pm\sigma_x + d_y^\pm\sigma_y$, with $d_x^\pm = \pm vq_x + t'\cos(k_z a/\sqrt{3})$ and $d_y^\pm = -vq_y + t'\sin(k_z a/\sqrt{3})$, where the velocity is defined as $v = \sqrt{3}ta/(2\sqrt{2})$, the small wave vector $\mathbf{q} = (q_x, q_y)$ is measured from $\pm\mathbf{K}$. By putting $d_{x,y}^\pm = 0$, we obtain the parametric equations of the spiral nodal lines around $\pm\mathbf{K}$ as $q_x = \mp(t'/v)\cos[(k_z a)/\sqrt{3}]$, $q_y = (t'/v)\sin[(k_z a)/\sqrt{3}]$, which have opposite chirality [Fig. 1(a)].

The nontrivial band topology of the NLSM is characterized by π Berry phase carried by each nodal line. The Hamiltonian H_0 possesses time reversal (T) symmetry, $H_0(\mathbf{k}) = TH_0(\mathbf{k})T^{-1} = H_0^*(-\mathbf{k})$, and inversion ($P$) symmetry, $H_0(\mathbf{k}) = PH_0(\mathbf{k})P^{-1} = \sigma_x H_0(-\mathbf{k})\sigma_x$, so that the Berry curvature vanishes everywhere away from the nodal

lines [72], and the nodal lines are protected by the combined PT symmetry [22]. Then one can choose an arbitrary integral path to calculate the Berry phase. Here we choose the integral path to be a straight line along the z direction, then the Zak phase calculated inside and outside the projection of the nodal line equals π and 0, respectively. This configuration of line integral is convenient to show the bulk-boundary correspondence of the NLSM, that is, DSS appear inside the projection of the nodal lines onto the surface Brillouin zone [Fig. 1(a)]. For a semi-infinite ($z < 0$) sample with an open surface lying at $z = 0$ [Fig. 1(d)], by substituting $k_z \to -i\partial_z$ in $h^\pm(\mathbf{q})$, the zero-energy DSS around $\mathbf{K}$, $\mathbf{K}'$ can be obtained as [24] $\psi_\pm \propto (0, 1)^{\text{T}} e^{\lambda_\pm z}$, where $\lambda_\pm = (\sqrt{3}/a)[\ln(t'/(v|\mathbf{q}|)) + i\theta_\pm]$, with $\theta_- = \tan^{-1}(q_y/q_x)$, $\theta_+ = \pi - \theta_-$. As long as $v|\mathbf{q}| < t'$, i.e., the states lie inside the projection of the nodal loops, the wave functions $\psi_\pm$ decays to zero as $z \to -\infty$, indicating the existence of sublattice polarized DSS [cf. 1(a)]; Otherwise, there are no surface states. The above results hold generally in the NLSM regime $t'/t < 1$. This can be checked by computing the band structure in a slab with the Hamiltonian H_0, infinite in the x-y plane and whose z axis lies along the (1,1,1) direction of the parent diamond lattice [inset of Fig. 1(d)]. We take a slab thick enough so that the two surfaces are decoupled, and we project the final result onto the upper half of the system to retain only the DSS on the upper surface. We show in Fig. 2(a) the band structure of the NLSM described above, where two pieces of zero-energy DSS exist. Without dispersion, the surface density of states (DOS) diverges at zero energy, see Fig. 2(b), whereas the bulk DOS vanishes.

Next, we include the SOC effect by second-neighbor hopping [73] as $H_{\text{SOC}} = i\lambda\sum_{\langle\langle i,j\rangle\rangle} c_i^\dagger \mathbf{s}\cdot(\mathbf{d}_{jk}\times\mathbf{d}_{ki})c_j$, where $c_i = (c_{i\uparrow}, c_{i\downarrow})$ is the Fermi operator for both spins on site i, λ is the SOC strength, $\mathbf{s}$ is the spin vector, and $\mathbf{d}_{ik}$ is the vector connecting sites i and k, and k is an intermediate site between i and j. The SOC term opens a gap in the band structure, both in the bulk and in the surface modes, lifting the spin degeneracy of the DSS [Fig. 2(c)] and introducing nontrivial spin textures to the DSS [Fig. 2(d)]. Its effect on the surface modes can be described by the following massive Dirac Hamiltonian $\mathcal{H}_{\text{SOC}}^\pm = \alpha(s_x q_y - s_y q_x) \pm \beta s_z$, with the superscript "$\pm$" corresponding to the $\mathbf{K}$ and $\mathbf{K}'$ points, which is sufficient to characterize the surface band topology [62]. Here, $\mathcal{H}_{\text{SOC}}^\pm$ is induced by the bulk SOC on an open surface, so that two coefficients $\alpha, \beta (>0)$ are determined by λ [62]. The parameter β introduces opposite mass terms to the DSS around the $\mathbf{K}$, $\mathbf{K}'$ points, see Fig. 1(b). Without SOC, the Hamiltonian for the DSS vanishes, so that $\mathcal{H}_{\text{SOC}}^\pm$ can serve as the effective Hamiltonian of the DSS. The Berry flux carried by each piece of DSS is calculated through $Q_\pm = [1/(4\pi)]\iint dq_x dq_y (\partial_{q_x}\mathbf{b}^\pm \times \partial_{q_y}\mathbf{b}^\pm)\cdot\mathbf{b}^\pm/|\mathbf{b}^\pm|^3$, with $\mathbf{b}^\pm = (\alpha q_y, -\alpha q_x, \pm\beta)$, yielding a topological charge, or meron
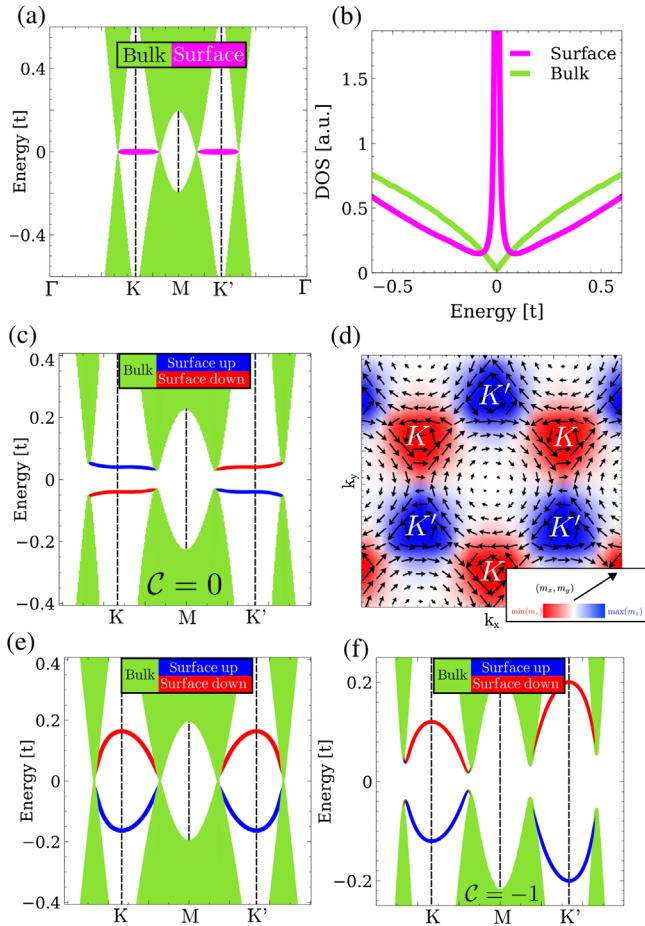
FIG. 2. (a) Band structure of a slab of a NLSM showing the surface flat bands. (b) Density of states (DOS) in the bulk and on the surface. (c) Band structure with only SOC. (d) Spin texture of the surface states. (e) Band structure with only interaction effect. (f) Band structure with both SOC and interaction effects. The slab consists of 600 layers and we took $t' = 0.8t$, $\lambda = 0.01t$, and $U = 2t$.

number [74] $Q_\pm = \pm\frac{1}{2}$ [75]. Each piece of DSS carries a meron number, but with an opposite sign, due to the opposite mass term. Two meron numbers thus cancel out and result in zero Chern number as imposed by time reversal symmetry. In this scenario, it is suggestive to think that, if one of the meron numbers would be inverted, the system would show a net Chern number [Fig. 1(c)].

We now show that electronic interactions can spontaneously break time reversal symmetry on the surface, inverting one of the meron number and turning the DSS into a Chern insulator. For that goal, it is convenient to first consider the case without SOC, where the system shows gapless flat DSS. In this situation, the infinite surface DOS would yield a Stoner ferromagnetic instability by arbitrarily small interaction, spontaneously breaking the time reversal symmetry on the surface. In contrast, for small U, no symmetry breaking occurs in the bulk states. The surface symmetry breaking can be captured

by adding an interaction term to the single particle Hamiltonian of the Hubbard form $H_U = U \sum_i n_{i\uparrow} n_{i\downarrow}$, with $n_{i\uparrow,\downarrow} = c^\dagger_{i\uparrow,\downarrow} c_{i\uparrow,\downarrow}$ the number operator. Taking magnetization along the z direction, in the mean-field picture the Hubbard interaction can be decoupled as $H_U \approx H_{MF} = U \sum_i [n_{i\uparrow}\langle n_{i\downarrow}\rangle + n_{i\downarrow}\langle n_{i\uparrow}\rangle - \langle n_{i\uparrow}\rangle\langle n_{i\downarrow}\rangle]$. The magnetization on site i is defined as $m_i^z = \langle n_{i\uparrow}\rangle - \langle n_{i\downarrow}\rangle$. The band structure of the self-consistent solution is shown in Fig. 2(e), with spin-polarized surface states and unpolarized bulk modes. In terms of the low energy model, electronic interaction results in an effective Zeeman term to the Hamiltonian for the DSS. In particular, at the K, K' points, the new term takes the form $\mathcal{H}_Z = -m_Z s_z$, where its strength can be evaluated as $m_Z = (U/2) \int_{-\infty}^0 m^z(z) |\psi_\pm(q = 0, z)|^2 dz$.

Finally, we consider the simultaneous action of both electronic interaction and SOC. By numerically solving the full self-consistent model with SOC, we observe that the surface magnetization survives even in the presence of SOC; see Fig. 2(f). In this situation, the effective Hamiltonian for the DSS takes the form $\mathcal{H} = \mathcal{H}_{SOC}^\pm + \mathcal{H}_Z$. Now the Chern number for the whole surface bands can be defined by the mass terms at the K, K' points as

$$\mathcal{C} = \frac{1}{2}[\text{sgn}(\beta - m_Z) + \text{sgn}(-\beta - m_Z)]. \quad (2)$$

As $m_Z > \beta$, the surface Zeeman splitting reverses the sign of the mass term around K [compare Figs. 2(c),2(f)], and drive the system to a Chern insulator [cf. Fig. 1(b)]. Such a kind of topological phase transition resembles the scenario of the Haldane model on the graphene lattice [76], yet here the sign change of the mass around one valley is dynamically generated by electronic interaction.

Since we are solving a self-consistent problem that does not have a smooth behavior, a gap closing and reopening cannot generically be observed. Nevertheless, since the mean-field term of the original Hamiltonian effectively reduces to a site-dependent exchange field that decays as one enters the bulk [Fig. 3(a)], we may try to artificially switch on its contribution, in order to adiabatically trace the topological phase transition. This can be made concrete by taking a final self-consistent Hamiltonian realizing the Chern insulating state $H = H_0 + H_{MF}$, and defining an adiabatic Hamiltonian of the form $\bar{H}(\alpha) = H_0 + \alpha H_{MF}$, where $\alpha = 0$ corresponds to the noninteracting Hamiltonian with $\mathcal{C} = 0$, whereas $\alpha = 1$ corresponds to the physical self-consistent solution with $\mathcal{C} = -1$. By tuning α from 0 to 1, the topological phase transition can be observed [Fig. 3(b)] as a gap closing and reopening in the energy spectra, concomitant with a change of Chern number from 0 to -1.

Since SOC opens up a gap in the single particle spectra, it is expected that at large values of λ the magnetic order will be quenched and the system will remain a trivial
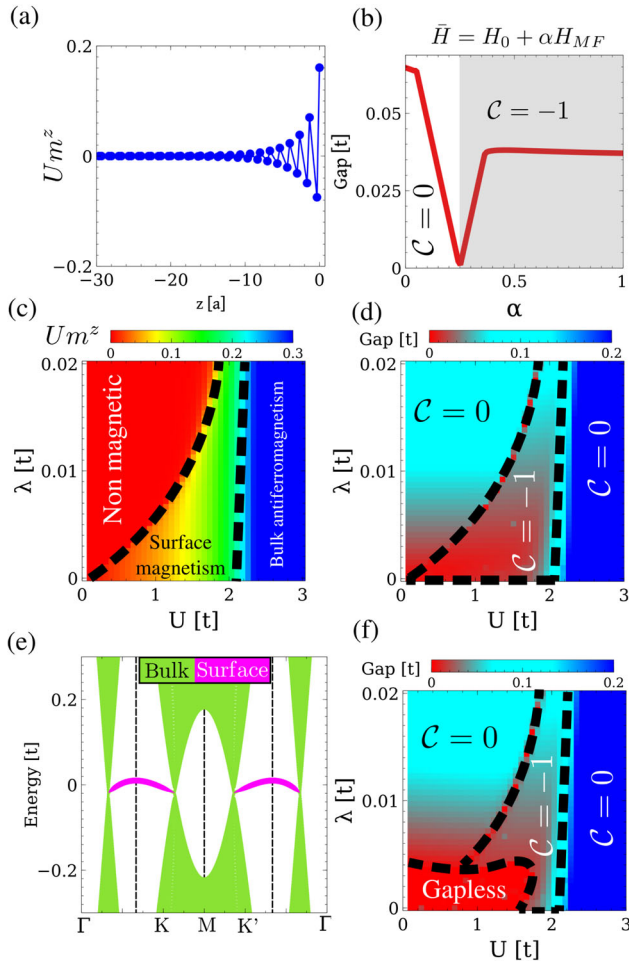
FIG. 3. (a) Real space distribution of the magnetization, where $z = 0$ corresponds to the surface. (b) Energy gap as a function of the mean-field order parameter. Phase diagram associated with (c) surface magnetization and (d) energy gap in terms of SOC strength λ and interaction U. (e) Band structure including the second-neighbor hopping $t_2 = 0.03t$, in the absence of U and λ. (f) Phase diagram containing chiral-symmetry breaking. We took $t' = 0.8t$, $\lambda = 0.01t$, and $U = 2t$ for (a),(b), 200 layers for (a),(b), (c),(d),(f) and 600 layers for (e).

semiconductor. This competition between SOC and electronic interaction is shown in the phase diagram in terms of U and λ in Figs. 3(c), 3(d). Different from the band closing and reopening by continuously tuning the order parameter in Fig. 3(b), the surface magnetization [Fig. 3(c)] and the energy gap [Fig. 3(d)] change abruptly with varying interaction U, indicating a phase transition with spontaneous symmetry breaking. Remarkably, such a conventional phase transition further induces and coincides with a topological phase transition on the surface. The topologically nontrivial phase with $\mathcal{C} = -1$ holds in a wide parametric region. For a larger λ, the parametric region of U for a Chern insulator becomes narrower, while the energy gap increases. For large U, the whole system becomes a trivial antiferromagnetic insulator, opening a large bulk magnetic gap.
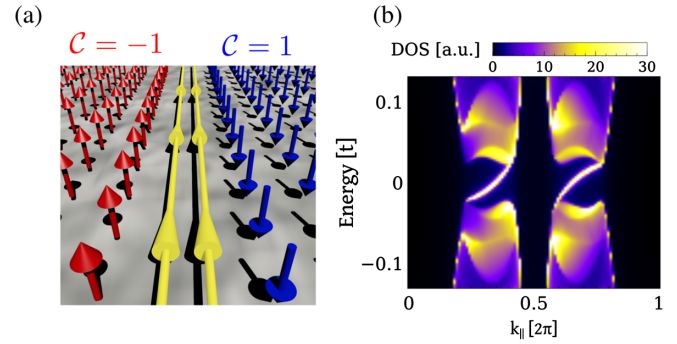

FIG. 4. (a) Sketch of the interfacial states in a magnetic domain wall on the surface of the NLSM. (b) Surface spectral function of the magnetic domain wall depicted in (a), showing two copropagating states along the domain wall.

The NLSM described by H_0 in Eq. (1) possesses chiral symmetry, $\sigma_z H_0 \sigma_z = -H_0$, which leads to flat DSS [70,77]. However, in real materials, chiral symmetry is usually broken, and the DSS show a finite dispersion. We investigate this situation by introducing a second-neighbor hopping to H_0. Dispersive DSS can be seen in the band structure in Fig. 3(e). The corresponding phase diagram in Fig. 3(f) shows a gapless region, yielding critical U and λ values for the onset of the surface Chern insulator. Apart from this, there is no much difference from the case of flat DSS.

A direct result of a 2D Chern insulator is the existence of chiral edge states. Here, the Chern insulator emerges on the surface of a 3D sample, resulting in chiral hinge states [Fig. 1(d)] [3–7,78–80]. The chiral edge states can also be achieved in a magnetic domain wall between two oppositely ordered ferromagnetic regions on the surface. The two regions are related by time reversal symmetry, so that they carry opposite Chern numbers, yielding a pair of chiral modes inside the domain wall; see Fig. 4(a). This image can be made concrete by computing the spectral function of the magnetic domain wall by means of the Dyson equation $G_D(\omega, k_\parallel) = [\omega - H_D(k_\parallel) - \Sigma_L(\omega, k_\parallel) - \Sigma_R(\omega, k_\parallel)]^{-1}$, where $k_\parallel$ is the Bloch momentum along the direction defined by the domain wall, $\Sigma_{L,R}(\omega, k_\parallel)$ are the self-energies induced by the semi-infinite magnetic regions (taken from the self-consistent solution of the infinite problem), and $H_D(k_\parallel)$ is the local Hamiltonian of the domain wall. With the previous Green's function, we compute the DOS at the surface as $(1/\pi)\text{Im}[\text{Tr}_U(G_D)]$, where Tr_U traces over the degrees of freedom of the upper surface. The interfacial spectral function is shown in Fig. 4(b), where it is seen that two gapless modes appear at the magnetic domain wall. Therefore, controlling such magnetic domain walls [81,82] would allow us to imprint chiral states on the surface of NLSMs.

To conclude, we have demonstrated that correlation effects and SOC can drive the NLSM into a surface Chern insulator. Spin-degenerate PT symmetric NLSMs

with two pieces of DSS in the surface Brillouin zone are potential candidates to achieve such a topological phase [62]. For the NLSM in the presence of SOC, since the nodal line is robust against SOC, other mechanisms are required to open a trivial gap in the bulk states [62].

[1] M. Z. Hasan and C. L. Kane, Rev. Mod. Phys. 82, 3045 (2010).
[2] X.-L. Qi and S.-C. Zhang, Rev. Mod. Phys. 83, 1057 (2011).
[3] W. A. Benalcazar, B. A. Bernevig, and T. L. Hughes, Science 357, 61 (2017).
[4] F. Schindler, A. M. Cook, M. G. Vergniory, Z. Wang, S. S. P. Parkin, B. A. Bernevig, and T. Neupert, Sci. Adv. 4, eaat0346 (2018).
[5] J. Langbehn, Y. Peng, L. Trifunovic, F. von Oppen, and P. W. Brouwer, Phys. Rev. Lett. 119, 246401 (2017).
[6] Z. Song, Z. Fang, and C. Fang, Phys. Rev. Lett. 119, 246402 (2017).
[7] C. M. Wang, H.-P. Sun, H.-Z. Lu, and X. C. Xie, Phys. Rev. Lett. 119, 136806 (2017).
[8] Z. Qiao, S. A. Yang, W. Feng, W.-K. Tse, J. Ding, Y. Yao, J. Wang, and Q. Niu, Phys. Rev. B 82, 161414 (2010).
[9] D. Xiao, W. Zhu, Y. Ran, N. Nagaosa, and S. Okamoto, Nat. Commun. 2, 596 (2011).
[10] K. Hamamoto, M. Ezawa, and N. Nagaosa, Phys. Rev. B 92, 115417 (2015).
[11] C.-X. Liu, S.-C. Zhang, and X.-L. Qi, Annu. Rev. Condens. Matter Phys. 7, 301 (2016).
[12] C.-Z. Chang et al., Science 340, 167 (2013).
[13] R. Yu, W. Zhang, H.-J. Zhang, S.-C. Zhang, X. Dai, and Z. Fang, Science 329, 61 (2010).
[14] C.-X. Liu, X.-L. Qi, X. Dai, Z. Fang, and S.-C. Zhang, Phys. Rev. Lett. 101, 146802 (2008).
[15] H. Weng, X. Dai, and Z. Fang, J. Phys. Condens. Matter 28, 303001 (2016).
[16] N. P. Armitage, E. J. Mele, and A. Vishwanath, Rev. Mod. Phys. 90, 015001 (2018).
[17] S. Murakami, New J. Phys. 9, 356 (2007).
[18] X. Wan, A. M. Turner, A. Vishwanath, and S. Y. Savrasov, Phys. Rev. B 83, 205101 (2011).
[19] H. Weng, C. Fang, Z. Fang, B. A. Bernevig, and X. Dai, Phys. Rev. X 5, 011029 (2015).
[20] S.-Y. Xu, C. Liu, S. K. Kushwaha, R. Sankar, J. W. Krizan, I. Belopolski, M. Neupane, G. Bian, N. Alidoust, T.-R. Chang, H.-T. Jeng, C.-Y. Huang, W.-F. Tsai, H. Lin, P. P. Shibayev, F.-C. Chou, R. J. Cava, and M. Z. Hasan, Science 347, 294 (2015).
[21] A. A. Burkov, M. D. Hook, and L. Balents, Phys. Rev. B 84, 235126 (2011).
[22] Y. Kim, B. J. Wieder, C. L. Kane, and A. M. Rappe, Phys. Rev. Lett. 115, 036806 (2015).
[23] R. Yu, H. Weng, Z. Fang, X. Dai, and X. Hu, Phys. Rev. Lett. 115, 036807 (2015).
[24] T. T. Heikkilä, N. B. Kopnin, and G. E. Volovik, JETP Lett. 94, 233 (2011).
[25] G. Xu, H. Weng, Z. Wang, X. Dai, and Z. Fang, Phys. Rev. Lett. 107, 186806 (2011).
[26] H. Weng, Y. Liang, Q. Xu, R. Yu, Z. Fang, X. Dai, and Y. Kawazoe, Phys. Rev. B 92, 045108 (2015).
[27] Y. Chen, Y. Xie, S. A. Yang, H. Pan, F. Zhang, M. L. Cohen, and S. Zhang, Nano Lett. 15, 6974 (2015).
[28] M. Zeng, C. Fang, G. Chang, Y.-A. Chen, T. Hsieh, A. Bansil, H. Lin, and L. Fu, arXiv:1504.03492.
[29] C. Fang, Y. Chen, H.-Y. Kee, and L. Fu, Phys. Rev. B 92, 081201 (2015).
[30] A. Yamakage, Y. Yamakawa, Y. Tanaka, and Y. Okamoto, J. Phys. Soc. Jpn. 85, 013708 (2016).
[31] L. S. Xie, L. M. Schoop, E. M. Seibel, Q. D. Gibson, W. Xie, and R. J. Cava, APL Mater. 3, 083602 (2015).
[32] Y.-H. Chan, C.-K. Chiu, M. Y. Chou, and A. P. Schnyder, Phys. Rev. B 93, 205132 (2016).
[33] J. Zhao, R. Yu, H. Weng, and Z. Fang, Phys. Rev. B 94, 195104 (2016).
[34] G. Bian, T.-R. Chang, H. Zheng, S. Velury, S.-Y. Xu, T. Neupert, C.-K. Chiu, S.-M. Huang, D. S. Sanchez, I. Belopolski, N. Alidoust, P.-J. Chen, G. Chang, A. Bansil, H.-T. Jeng, H. Lin, and M. Z. Hasan, Phys. Rev. B 93, 121113 (2016).
[35] G. Bian et al., Nat. Commun. 7, 10556 (2016).
[36] T. Bzdušek, Q. Wu, A. Rüegg, M. Sigrist, and A. A. Soluyanov, Nature (London) 538, 75 (2016).
[37] Q. Yan, R. Liu, Z. Yan, B. Liu, H. Chen, Z. Wang, and L. Lu, Nat. Phys. 14, 461 (2018).
[38] W. Chen, H.-Z. Lu, and J.-M. Hou, Phys. Rev. B 96, 041102 (2017).
[39] Z. Yan, R. Bi, H. Shen, L. Lu, S.-C. Zhang, and Z. Wang, Phys. Rev. B 96, 041103 (2017).
[40] M. Ezawa, Phys. Rev. B 96, 041202 (2017).
[41] R. Bi, Z. Yan, L. Lu, and Z. Wang, Phys. Rev. B 96, 201305 (2017).
[42] Z. Yan and Z. Wang, Phys. Rev. Lett. 117, 087402 (2016).
[43] Z. Yan and Z. Wang, Phys. Rev. B 96, 041206 (2017).
[44] Y. Du, F. Tang, D. Wang, L. Sheng, E.-j. Kan, C.-G. Duan, S. Y. Savrasov, and X. Wan, Quantum Mater. 2, 3 (2017).
[45] Q. Xu, R. Yu, Z. Fang, X. Dai, and H. Weng, Phys. Rev. B 95, 045136 (2017).
[46] H. Huang, J. Liu, D. Vanderbilt, and W. Duan, Phys. Rev. B 93, 201114 (2016).
[47] X. Zhang, Z.-M. Yu, X.-L. Sheng, H. Y. Yang, and S. A. Yang, Phys. Rev. B 95, 235116 (2017).
[48] N. B. Kopnin, T. T. Heikkilä, and G. E. Volovik, Phys. Rev. B 83, 220503 (2011).
[49] J. Liu and L. Balents, Phys. Rev. B 95, 075426 (2017).
[50] B. Pamuk, J. Baima, F. Mauri, and M. Calandra, Phys. Rev. B 95, 075422 (2017).

[51] T. Löthman and A. M. Black-Schaffer, Phys. Rev. B **96,** 064505 (2017).

[52] B. Roy, Phys. Rev. B **96,** 041113 (2017).

[53] M. Slota et al., Nature (London) **557,** 691 (2018).

[54] M. Fujita, K. Wakabayashi, K. Nakada, and K. Kusakabe, J. Phys. Soc. Jpn. **65,** 1920 (1996).

[55] K. Wakabayashi, M. Fujita, H. Ajiki, and M. Sigrist, Phys. Rev. B **59,** 8271 (1999).

[56] Y.-W. Son, M. L. Cohen, and S. G. Louie, Nature (London) **444,** 347 (2006).

[57] C. Fang, H. Weng, X. Dai, and Z. Fang, Chin. Phys. B **25,** 117106 (2016).

[58] Y. Chen et al., Science **329,** 659 (2010).

[59] L. A. Wray, S.-Y. Xu, Y. Xia, D. Hsieh, A. V. Fedorov, Y. San Hor, R. J. Cava, A. Bansil, H. Lin, and M. Z. Hasan, Nat. Phys. **7,** 32 (2011).

[60] M. Mogi, M. Kawamura, A. Tsukazaki, R. Yoshimi, K. S. Takahashi, M. Kawasaki, and Y. Tokura, Sci. Adv. **3,** eaao1669 (2017).

[61] D. Xiao et al., Phys. Rev. Lett. **120,** 056801 (2018).

[62] See Supplemental Material at http://link.aps.org/supplemental/10.1103/PhysRevLett.122.016803 for the derivation of surface spin-orbit coupling, mean field calculations, discussion on the ferromagnetic order and the direction of magnetization, the nodal line semimetals with spin-orbit coupling, and possible material realizations, which includes Refs. [12,22,25,29,32,44–47,49,57,63–68].

[63] E. H. Lieb, Phys. Rev. Lett. **62,** 1201 (1989).

[64] Q. Liu, C.-X. Liu, C. Xu, X.-L. Qi, and S.-C. Zhang, Phys. Rev. Lett. **102,** 156603 (2009).

[65] D. A. Abanin and D. A. Pesin, Phys. Rev. Lett. **106,** 136802 (2011).

[66] J. McClure, Carbon **7,** 425 (1969).

[67] Y. Henni, H. P. Ojeda Collado, K. Nogajewski, M. R. Molas, G. Usaj, C. A. Balseiro, M. Orlita, M. Potemski, and C. Faugeras, Nano Lett. **16,** 3710 (2016).

[68] M. G. Brik, A. Suchocki, and A. Kaminska, Inorg. Chem. **53,** 5088 (2014).

[69] J. McClure, Carbon **7,** 425 (1969).

[70] T. Hyart, R. Ojajärvi, and T. T. Heikkilä, J. Low Temp. Phys. **191,** 35 (2018).

[71] J. L. Lado and M. Sigrist, Phys. Rev. Lett. **121,** 037002 (2018).

[72] L. Fu and C. L. Kane, Phys. Rev. B **76,** 045302 (2007).

[73] L. Fu, C. L. Kane, and E. J. Mele, Phys. Rev. Lett. **98,** 106803 (2007).

[74] B. A. Bernevig and T. L. Hughes, Topological Insulators and Topological Superconductors (Princeton University Press, Princeton, NJ, 2013).

[75] The meron number will be half-quantized only in the low energy limit, when the mass term is much smaller than the nonlinear corrections to the dispersion, so that the Berry curvature is heavily concentrated around the K, K' points.

[76] F. D. M. Haldane, Phys. Rev. Lett. **61,** 2015 (1988).

[77] S. Ryu and Y. Hatsugai, Phys. Rev. Lett. **89,** 077002 (2002).

[78] M. Sitte, A. Rosch, E. Altman, and L. Fritz, Phys. Rev. Lett. **108,** 126807 (2012).

[79] F. Zhang, C. L. Kane, and E. J. Mele, Phys. Rev. Lett. **110,** 046404 (2013).

[80] L. Li, H. H. Yap, M. A. N. Araújo, and J. Gong, Phys. Rev. B **96,** 235424 (2017).

[81] T. H. E. Lahtinen, K. J. A. Franke, and S. van Dijken, Sci. Rep. **2,** 258 (2012).

[82] L. J. McGilly, P. Yudin, L. Feigl, A. K. Tagantsev, and N. Setter, Nat. Nanotechnol. **10,** 145 (2015).